Received 27 October 2023; revised 7 December 2023; accepted 31 December 2023. Date of publication 5 January 2024; date of current version 29 January 2024.
The review of this article was arranged by Editor Z. Zhang.

Digital Object Identifier 10.1109/JEDS.2024.3350230

Potentiometric MgO Film pH Sensor Measurement Analysis and Integrated Flexible Printed Circuit Board

PO-HUI YANG (Member, IEEE), JYUN-MING HUANG, YING-SHENG CHANG, CHE-TSUNG CHAN, AND WEI-SHUN CHEN

Graduate School of Electronic Engineering, National Yunlin University of Science and Technology, Douliou 64002, Taiwan

CORRESPONDING AUTHOR: P.-H. YANG (e-mail: phyang@yuntech.edu.tw)

This work was supported by the National of Science and Technology Council, Republic of China, under Contract NSTC 111-2221-E-224-058 and Contract NSTC 112-2221-E-224-049.

ABSTRACT In recent years, research in the field of sensors has been rapidly advancing. As a result, this study proposes a pH sensor based on a magnesium oxide (MgO) thin film. The MgO sensing layer of the pH sensor was deposited onto the electroless nickel immersion gold (ENIG) electrode using a radio frequency (RF) sputtering system, where the ENIG electrode is integrated as the working electrode and reference electrode on a Flexible Printed Circuit Board (FPCB). FPCB offers advantages such as flexibility, acid resistance, heat resistance, and low cost. Furthermore, the performance of the pH sensor is enhanced by modifying the sensing layer with Nafion and (3-Aminopropyl)triethoxysilane (APTES). This study utilized the potentiometric method to measure and analyze the performance of the pH sensor, and the measurement range of the pH sensor is from pH 3 to pH 11 with an average sensitivity of 46.48 mV/pH and linearity can reach 0.996. In terms of material analysis, this research utilizes atomic force microscopy (AFM) and energy dispersive X-ray spectroscopy (EDX) to analyze the surface morphology and elemental composition of the sensing layer to verify MgO film.

INDEX TERMS Magnesium oxide (MgO), pH sensor, flexible printed circuit board (FPCB), electroless nickel immersion gold (ENIG) electrode, instrumentation amplifier (INA).

I. INTRODUCTION

The development of pH sensing components began in 1970 [1]. In recent developments, pH sensors have found wide applications in fields such as agriculture [2], healthcare [3], food processing [4], and environmental safety testing [5], so the development of pH sensors is crucial. However, many sensors have different sensing structures, such as ion-sensitive field-effect transistors (ISFET), extended-gate field-effect transistors, and electrolyte-insulator-semiconductor (EIS) devices [6]. Gaddour et al. [7]. proposed a temperature-compensated ISFET that reduces the influence of temperature when detecting pH value. Pan et al. [8]. analyzed the effects of different indium (In) content in pH sensors on sensitivity, drift rate, and hysteresis voltage using the EGFET structure. Kao et al. [9]. prepared Mg-doped IGZO sensing layers on the EIS structure using sputtering and analyzed the performance of the sensor for H^+, Na^+, and K^+ measurements.

These structures often lack flexibility, this point is an important factor in sensor fields. Hence, this study utilizes a flexible printed circuit board (FPCB) as the substrate for the sensor. FPCB offers several advantages, including flexibility, lightweight, acid and heat resistance, and the ability for mass production [10]. FPCB consists of a polyimide (PI) base, copper (Cu) conductors, and working and reference electrodes made using a chemical process known as electroless nickel immersion gold (ENIG). ENIG is a surface treatment technique that involves depositing a layer of nickel followed by a layer of gold on a metal surface [11]. This technology is commonly used to enhance the appearance of metal surfaces and improve their corrosion resistance, wear resistance, and conductivity. ENIG working electrodes have a smooth surface, which is beneficial for

© 2024 The Authors. This work is licensed under a Creative Commons Attribution 4.0 License.
For more information, see https://creativecommons.org/licenses/by/4.0/

ensuring that the sensing layer remains flat during the sputtering process, without defects. It also helps maintain the stability of their sensing properties.

Among the many pH sensors, metal oxides are often chosen as the sensing layer, such as Ruthenium Oxide (RuO_x), iridium oxide (IrO_x), zinc oxide (ZnO), and Titanium oxide (TiO_2). Tanumihardja et al. [12] presented a potentiometric pH sensor with RuO_x nanorods, which features low drift and a fast response time. Huang et al. [13] used the sol-gel method to prepare IrO_x thin film on a polymer substrate and investigated the pH sensor's sensitivity, response time, repeatability, and selectivity. Srikanya et al. [14] reported a double-gate ZnO thin film ISFET for pH sensing, which exhibits an enhanced voltage sensitivity of 205.57 mV/pH. Yang et al. [15] employed a hydrothermal method to create TiO_2 nanoflower structures on a fluorine-doped tin oxide substrate for an EGFET, achieving a sensitivity of 46 mV/pH and a linear response of 0.998. Metal oxide has unique electrical, and electrochemical characteristics, and a high surface area to volume ratio, enhancing the sensor's sensitivity and catalytic properties [1].

Therefore, in the selection of sensing layer materials, this study chose a low-cost and commonly used material. Magnesium oxide (MgO) is a metal oxide that finds application in various fields [16], [17], [18]. It is widely used in the industrial sector for refractory materials. In the field of electrochemistry, it is applied in fuel cells. In the medical field, MgO is used in pharmaceutical preparation. Additionally, MgO exhibits excellent optical and electrical properties and is widely employed in optical instruments, lasers, semiconductor devices, and other areas. Furthermore, MgO is an inorganic compound with a perovskite structure and a high energy bandgap of 7.8 eV [19].

Considering these advantages and characteristics, this study is grounded in developing a novel pH sensor using flexible sensors, specifically employing FPCB. The selected pH sensor substrate exhibits characteristics of heat resistance, acid resistance, and flexibility. Additionally, it incorporates a MgO sensing layer, offering advantages such as non-toxicity, residue-free properties, and ease of absorption by the human body [20]. This design imparts significant versatility to the sensor, rendering it highly adaptable for applications in the biomedical field, environmental safety, and industrial settings.

In the biomedical domain, this pH sensor finds application in monitoring physiological fluids. Simultaneously, the sensor can be utilized for water quality monitoring in environmental safety, contributing to environmental protection efforts. Furthermore, its widespread application in the industrial sector includes detection within chemical production processes, exemplifying its utility in industrial applications.

This study employs a potentiometric voltage-time (V-T) measurement system. The measurement system comprises an instrumentation amplifier (INA), data acquisition (DAQ) system, and LabView software to analyze the characteristics of pH sensing capability. These characteristics include low drift, low DC offset, high input impedance, and a very large common-mode rejection ratio (CMRR) [21]. However, we refer to the potential difference output by the IA as the response voltage and then analyze the sensing capability of the pH sensor based on this response voltage.

TABLE 1. The fabrication method of the pH solution.

Solution **A**	Citric Acid 1.4409 (g)	Boric Acid 1.8549 (g)	D. I. water 150(mL)
Solution **B**	Sodium Phosphate Tribasic 12-hydrate 5.7021 (g)		D. I. water 150(mL)
pH value	Solution **A** volume (mL)	Solution **B** volume (mL)	
3	44.00	06.00	
5	33.50	16.50	
7	24.75	25.25	
9	17.25	32.75	
11	11.00	39.00	

II. EXPERIMENTS

A. THE MATERIALS OF THE EXPERIMENT

This study used a 2-inch MgO target to fabricate MgO film through an RF sputtering system as the sensing layer. Subsequently, Nafion and APTES were modified on the MgO sensing layer using a drop-casting method. Both Nafion and APTES were purchased from Sigma-Aldrich Co. (USA). The sensor substrate was fabricated in bulk by a commissioned professional PCB manufacturer, Rui Xing Circuit Co., Ltd. (China).

The pH solution used in the experiments was fabricated by Carmody's wide-range buffer solution [22]. Firstly, A solution and B solution were prepared, as shown in Table 1. A solution was prepared by mixing 0.05 M citric acid, 0.2 M boric acid, and 150 mL of deionized water. B solution was prepared by mixing 0.1 M sodium phosphate tribasic 12-hydrate and 150 mL of deionized water. Both A and B solutions were placed in an ultrasonic bath and subjected to ultrasonication until the powders were completely dissolved in water. Then, the two solutions were mixed in the proportions indicated in Table 1. The pH of the resulting solution was verified using a pH detector to ensure accuracy.

B. FABRICATION OF THE NAFION/APTES/MGO SENSING LAYER

First, this study follows a series of steps to ensure the thorough cleaning of the ENIG surface on the FPCB to guarantee the high quality of the sensing film. This cleaning process involves the use of alcohol, acetone, and deionized water to effectively remove surface contaminants. Next, we used the MgO target (99%) through an RF sputtering system to fabricate the MgO sensing layer on the working electrode. Table 2 provides the sputtering parameters for the MgO film, including a gas ratio set at 10:2 (sccm), sputtering power set at 60 watts, and deposition for 30 minutes under low-pressure

TABLE 2. Sputtering parameters of the MgO sensing layer.

Target	Gas flow ratio (Ar: O_2)	RF power	Deposition pressure	Deposition time
MgO (99 %)	10:2 (sccm)	60 W	3 mTorr	30 minutes

conditions (3 mTorr). This process ensures the consistency and stability of the MgO film to provide reliable sensing performance. Finally, we employ a drop-casting method to further enhance the characteristics of the sensing layer. Firstly, we sequentially add 2 μL of APTES (1 wt%) and 2 μL of Nafion (5 wt%), which improve the layer's sensing performance. It is worth noting that during the modification process, we adopt a lower temperature approach to drying the modified layer under conditions of 70 °C to ensure the stability and uniformity of the modification layer.

C. THE PH SENSOR STRUCTURE AND POTENTIOMETRIC MEASUREMENT SYSTEM

In this chapter, we will begin discussing the structure and dimensions of the pH sensor. Figure 2 shows the composition of the working electrode and the reference electrode. First, the pH sensor employs an FPCB as its substrate. The substrate is composed of polyimide and copper is used as the wiring to connect the working electrode and reference electrode. The entire FPCB electrode surface is coated with an ENIG layer, as shown in Figure 2(a). However, the sensing layer of the pH sensor is depicted in Figure 2(b-c). The MgO sensing layer in Figure 2(b) is prepared using an RF sputtering system. Figure 2(c-d) represents APTES and Nafion, both of which are modification layers created using the drop-casting method.

This study enhances the pH sensor's sensing performance through the modification layer of the APTES and Nafion [23], [24], [25]. Regarding electrode dimensions, the working electrode has an area of 3.14 mm^2, and the reference electrode has an area of 22 mm^2.

This study employs a potentiometric method to measure and analyze the capabilities of the pH sensor. This potentiometric method analyzes the voltage generated per second, which we refer to as the voltage-time (V-T) measurement system. First, the pH sensor is connected to a readout circuit consisting of a commercial IC, LT1167. The LT1167 is composed of an Instrumentation Amplifier (INA), and the measurement is carried out with a gain (Av) of one. The V+ and V− pins of the INA are connected to the working electrode and reference electrode, respectively. The potential difference generated between these two electrodes is used to analyze the measured pH value, where the potential difference is referred to as the response voltage in this study.

Subsequently, the analog signal is converted into a digital signal by the analog-to-digital converter (ADC) of the data acquisition system (DAQ). The DAQ then transmits the signal to the LaView software for the presentation of measurement data. The measurement environment is shown in Figure 1.

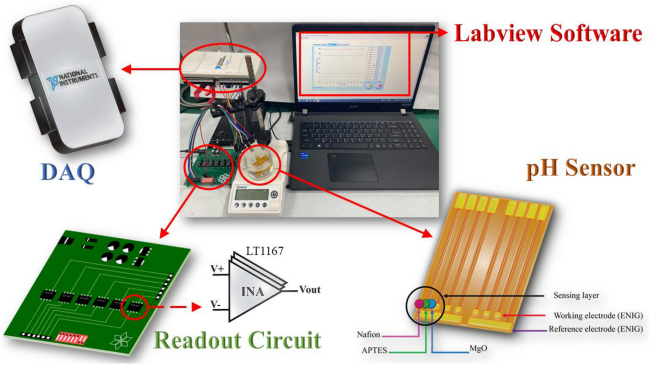

FIGURE 1. The measurement environment of the Nafion/APTES/MgO pH sensor.

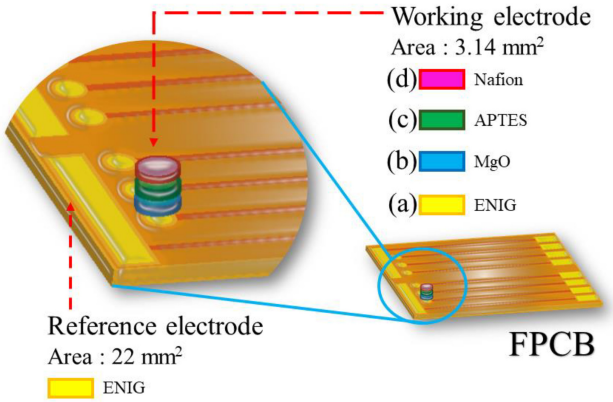

FIGURE 2. The structure of the Nafion / APTES / MgO / ENIG / Cu / PI pH sensor, (a) Nafion, (b) APTES, (c) MgO, (d) ENIG.

III. RESULTS AND DISCUSSION

A. AFM AND EDX ANALYSIS OF THE MAGNESIUM OXIDE CHARACTERISTIC

This study employed an Atomic Force Microscope (AFM) to analyze the surface morphology and roughness of MgO. The AFM instrument used was the Dimension ICON XR (USA). In this chapter, we will discuss the surface morphology of MgO films deposited on both silicon substrates (MgO/Si) and FPCB substrates (MgO/ENIG/Cu/PI) after AFM analysis. The scanning area for AFM analysis was 25 μm^2.

Furthermore, this study conducted an analysis of the surface roughness of the MgO films, including Root Mean Square roughness (R_{rms}), Average roughness (R_a), and the highest roughness height (R_h). The analysis results are shown in Figures 3 and 4, including both 2D and 3D analyses. In the analysis of MgO/Si, R_{rms}, R_a, and R_{max} were 1.44 nm, 1.04 nm, and 15.3 nm, respectively. In the analysis of MgO/ENIG/Cu/PI, R_{rms}, R_a, and R_h were 12.6 nm, 10.1 nm, and 91.7 nm, respectively.

Based on the analysis results, it is evident that the R_{ms} of MgO/ENIG/Cu/PI is much rougher compared to

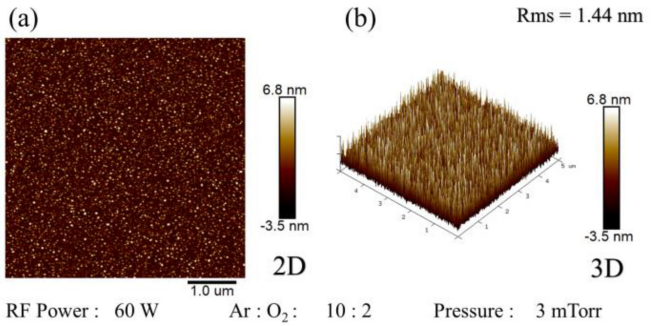

FIGURE 3. The AFM analysis of the MgO film deposited on the silicon wafer, the scan area is 25 μm^2, (a) 2D and (b) 3D morphological images.

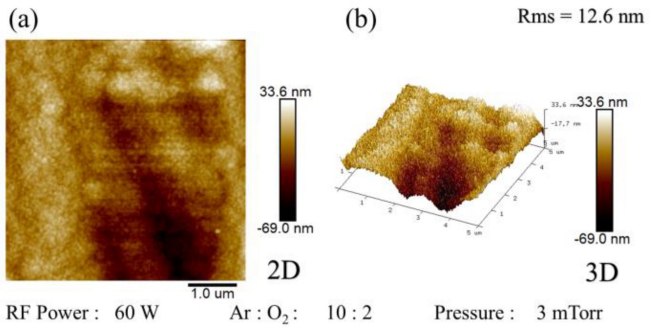

FIGURE 4. The AFM analysis of the MgO film deposited on the FPCB, the scan area is 25 μm^2, (a) 2D and (b) 3D morphological images.

MgO/Si, primarily due to different surface stresses on the substrates during sputtering, resulting in distinct morphologies. Notably, the roughness of the film varies depending on the substrate material, as seen in the AFM analysis results. Additionally, to corroborate the AFM analysis, this study used Energy-Dispersive X-ray Spectroscopy (EDX) to confirm the elemental composition of the film as MgO. The EDX analysis results, as shown in Figure 5, indeed confirm the presence of both Mg and O elements in the film.

B. SENSING MECHANISM BETWEEN MGO AND PH SENSOR

In chemical sensor technology, scientists are dedicated to in-depth studies of the charging behavior of metal oxides in electrolyte solutions, with a simultaneous focus on the impact of pH values in electrolyte solutions on electrostatic potential. Hiemstra et al. [26] have proposed a theoretical framework named the multiplesite complexation model (MUSIC) to elucidate the charging mechanism of oxides. This model integrates concepts from the site dissociation and one-pK models, utilizing physical parameters to estimate the intrinsic dissociation constants of active surface groups. Notably, the inherent dissociation constants of these groups are influenced by various factors, including the oxidation state of metal ions, the number of ligand cations, and the number of ligands surrounding the metal ions. Additionally, these factors have specific effects on different reactive groups present in specific oxides [27], [28].

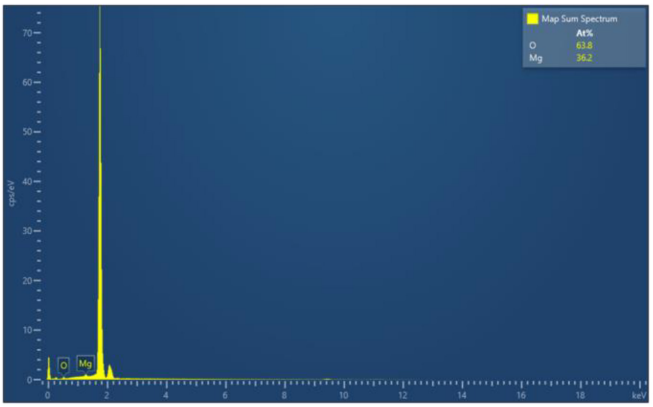

FIGURE 5. The EDX analysis of the MgO film.

MgO is an alkaline oxide, playing a crucial role as an electron donor in aqueous solutions, and its surface undergoes protonation and deprotonation [29], [30], [31], [32]. However, when MgO comes into contact with an aqueous solution, OH^- anions are adsorbed onto the positively charged surface of MgO. These OH^- anions eventually desorb from the surface, releasing magnesium ions into the solution. As this process continues, the ion concentration in the solution gradually reaches a state of oversaturation, at which point hydroxides begin to precipitate on the oxide surface. Formulas (1 - 4) describe the chemical behavior of MgO in water and emphasize its importance in electron transfer and anion adsorption.

$$MgO + H_2O \rightarrow MgOH^+ + OH^- \quad (1)$$
$$MgOH^+ + OH^- \rightarrow MgOH^+ \cdot OH^- \quad (2)$$
$$MgOH^+ \cdot OH^- \rightarrow Mg^{2+} + 2OH^- \quad (3)$$
$$Mg^{2+} + 2OH^- \rightarrow Mg(OH)_2 \quad (4)$$

C. SENSING PERFORMANCE OF THE NAFION/APTES/MGO PH SENSOR

In sensor research, linearity and average sensitivity are important indicators. The former refers to the measurement precision and accuracy of the sensor, while the latter represents the minimum or maximum concentration that the sensor can detect and is used to assess the sensitivity of the sensor measurement range. This study analyzes the performance of the sensor by examining the response voltage generated when a pH sensor is immersed in different pH values.

Figure 6 shows the results of measurements taken with the Nafion/APTES/MgO pH sensor. This sensor has an average sensitivity of 46.48 mV/pH and achieves a linearity of 0.996. According to the measurement results, the sensor modified with APTES does indeed exhibit excellent sensitivity. This is due to the protonation and deprotonation of the working electrode surface, which enhances the sensor's electron transfer and anion adsorption capabilities [21], resulting in improved linearity and sensitivity.

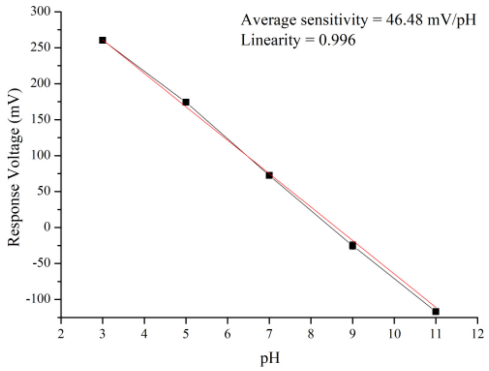

FIGURE 6. The performance of the Nafion/APTES/MgO pH sensor.

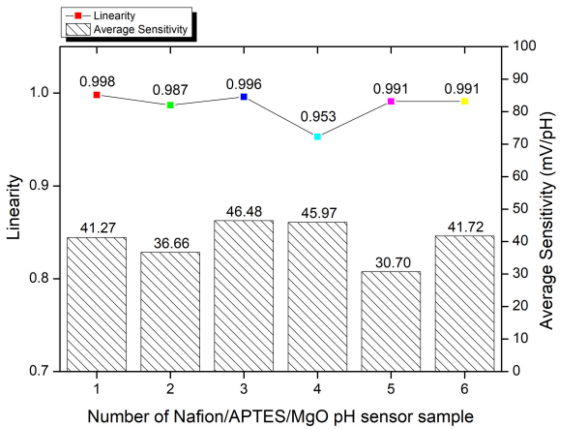

FIGURE 7. The reproducibility of the Nafion/APTES/MgO pH sensor.

D. REPRODUCIBILITY OF THE NAFION/APTES/MGO PH SENSOR

The purpose of the reproducibility experiment was to assess the stability and reliability of the Nafion/APTES/MgO pH sensor during the manufacturing process. To achieve this objective, we conducted a series of reproducible experiments. These experiments include the measurement and analysis of six sets of pH sensors within a pH range of 3 to 11.

Firstly, the pH sensor was immersed in a pH solution with varying pH concentrations, and we measured and recorded the response voltage for each pH value. This allowed us to calculate the average sensitivity and linearity for each set of sensors. The relative standard deviation (RSD) was then computed based on the average sensitivity and linearity values of each sensor group, as specified in the formula (6), where "S" represents the mean value of average sensitivity, and "x" represents the standard deviation of average sensitivity.

The results of these measurements are presented in Figure 7, showing that the RSD value for the pH sensors is 7.83%. Despite the potential for variations in the manufacturing process to impact average sensitivity and linearity, the calculated RSD results highlight the outstanding stability and reliability of the Nafion/APTES/MgO pH sensor.

$$\mathrm{RDS} = \frac{s}{\bar{x}} \times 100\% \tag{5}$$

E. RESPONSE TIME OF THE NAFION/APTES/MGO PH SENSOR

When the surface of the working electrode comes into contact with a pH solution, the pH sensor reacts with the H^+ in the solution to generate a potential difference. Over time, the response voltage of the sensor gradually approaches stability. Therefore, we selected 95% of the stable voltage as the termination point of the response time [33] to ensure that the measured response time is sufficiently reliable and accurate. In this experiment, we also further tested the response time at different pH values to compare the measurement characteristics at different pH values, which helps to further verify the sensing performance of the Nafion/APTES/MgO pH sensor. In this study, we immersed the sensor in 1 mL of pH 7 neutral solution and then dropped 200 μL of acidic and alkaline solutions separately, where the pH values of the acidic and alkaline solutions were pH 3 and pH 11, respectively. The purpose of this experiment was to observe how long it takes for the response voltage to reach a stable state when the pH of the solution changes while the sensor is placed in the pH 7 neutral solution.

According to the experimental results, we use formula 1 and formula 2 to calculate the response time measured by the two methods, and the measured time is 5 s and 6 s, it can be seen from the experimental results that when the sensor When immersed in a neutral solution and changes to alkaline or acidic, the response voltage can quickly reach a steady state, so it has a fast response time, and the results are shown in Figure 8.

$$V_R = V_I + (V_S - V_I) \times 95\ \% \tag{6}$$

$$Rt = t_{VR} - t_{VI} \tag{7}$$

Formula (6) calculates the 95% response voltage (V_R), where V_I is the initial stable response voltage and V_S is the final stable response voltage. Formula (7) calculates the response time (R_t), where t_{VR} is the time to 95% response voltage and t_{VI} is the time to initial response voltage.

F. INTERFERENCE EFFECTS OF THE NAFION/APTES/MGO PH SENSOR

In this study, we conducted interference tests to examine whether the Nafion/APTES/MgO pH sensor is susceptible to interference from other ions, specifically K^+ and Na^+ ions. During the testing process, we initially immersed the pH sensor in a PBS solution and waited for the response voltage to stabilize. We added 200 μL of NaCl and KCl solutions to a PBS solution with a pH of 7 at 50-second intervals, where the concentration of NaCl and KCl solutions is 0.1 M. The results of the measurements and analysis are presented in Figure 9.

The analysis in this experimental method is based on the voltage difference resulting from the addition of

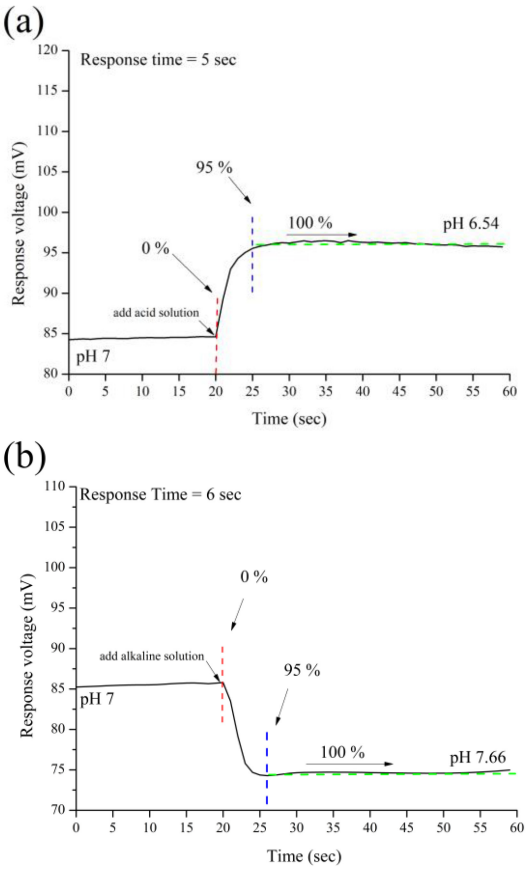

FIGURE 8. The response time of the Nafion/APTES/MgO pH sensor, (a) a neutral solution turns into an acidic solution, (b) a neutral solution to an alkaline solution.

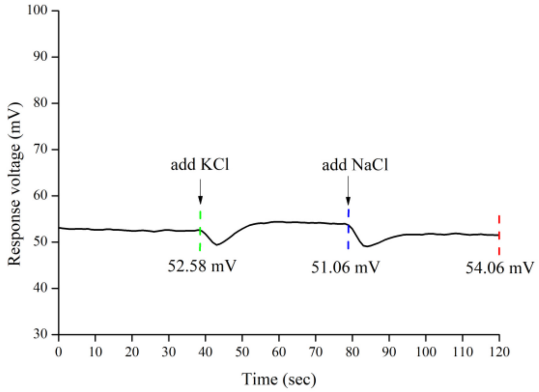

FIGURE 9. The interference effect of the Nafion / APTES / MgO pH sensor.

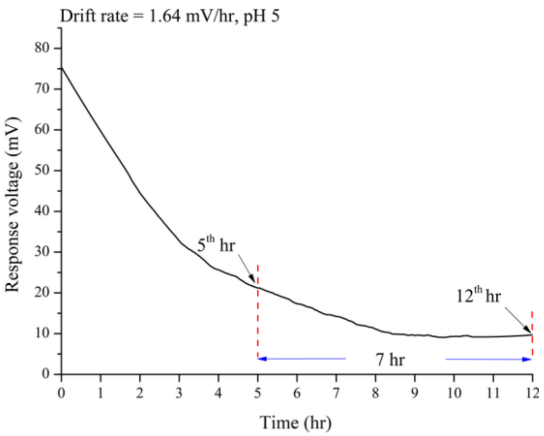

FIGURE 10. The time drift of the Nafion/APTES/MgO pH sensor in pH 5 solution.

ion interferences, which allows us to assess the sensor's interference resistance. According to the results in Figure 9, we observed that the potential changes when adding NaCl and KCl were 3 mV and 1.12 mV, respectively. These changes represented only a 5.5% and 3.8% variation, respectively.

These findings suggest that the Nafion/APTES/MgO pH sensor is minimally affected by interference from Na^+ and K^+ ions and demonstrates good interference resistance, indicating its suitability for accurate pH measurements in the presence of these ions.

G. DRIFT EFFECT OF THE NAFION/APTES/MGO PH SENSOR

The drift effect in time is a non-ideal phenomenon representing the stability of a sensor during long-term measurements [34]. When a sensor is immersed in the test solution for an extended period, the response voltage changes over time, and this phenomenon is known as drift [35]. The reason for this occurrence is the formation of hydroxyl groups on the sensor film's surface, and the polar molecules in the solution result in the diffusion of hydration ions, formed by Coulombic attraction, onto the sensor membrane, creating a hydration layer. The variation in the surface potential of the sensor membrane is attributed to the double-layer capacitance of the hydration layer.

In this study, it was observed that the variation in the first 5 hours of long-term measurements is larger compared to the subsequent 7 hours. This is because the hydration layer on the surface of the sensing film has not fully formed, leading to a greater variation in response voltage. Consequently, we define the drift effect as the difference between the output response voltage at the 5^{th} hour and the 12^{th} hour, divided by 7 to obtain the hourly drift rate, as shown in formula 8. A drift rate closer to 0 indicates better stability of the sensor. Therefore, this experiment can be regarded as a stability measurement of the sensor.

This study immersed the fabricated Nafion/APTES/MgO pH sensor in pH 5 and pH 9 solutions for a continuous 12-hour measurement. Figure (10 - 11) presents the results of the drift rate. In the results of this study, the drift rate in the acidic solution was 1.64 mV/hr, and in the alkaline solution, it was 0.88 mV/hr, both exhibiting lower hourly drift rates. Hence, the sensor demonstrates good stability in both acidic and alkaline solutions. However, it was observed that the Nafion/APTES/MgO pH sensor exhibited different

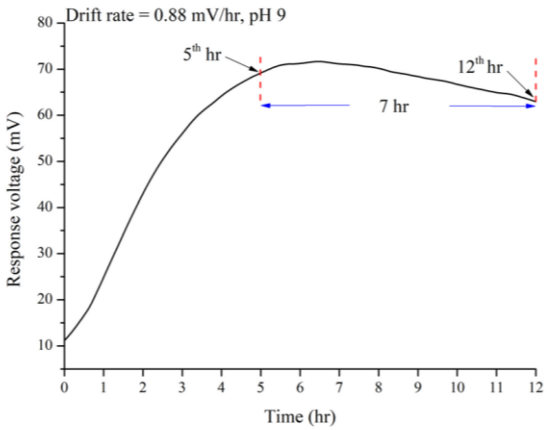

FIGURE 11. The time drift of the Nafion/APTES/MgO pH sensor in pH 9 solution.

directions of response voltage drift when subjected to long-term measurements in acidic and alkaline solutions due to protonation and deprotonation of the sensing electrode.

$$\text{Drift rate} = \frac{V_{12th} - V_{5th}}{7} \tag{8}$$

H. STABILITY OF SENSING ELECTRODE

In this research, the working electrode functions to react with the test solution, while the reference electrode provides a stable response voltage as a reference point. Therefore, this study further investigates the stability of the Nafion/APTES/MgO pH sensor's sensing electrode during the measurement process. Initially, the study measured the response voltage at pH 3, pH 7, and pH 11. This process was repeated ten times, and the response voltage was recorded each time. Figure 12 illustrates these results. We calculated the RSD based on Formula 5 to evaluate the sensor's performance further. In Formula 5, S represents the standard deviation of the response voltage over ten measurements, and x represents the average of the ten response voltages. According to our calculations, the RSD values for pH 3, pH 7, and pH 11 were 1.4%, 0.8%, and 0.5%, respectively. Figure 12 shows that under pH 3, pH 7, and pH 11 conditions, the pH sensor exhibits relatively stable characteristics. It demonstrates the excellent repeatability of the Nafion/APTES/MgO pH sensor and the sensing electrode's stability, affirming the sensor's reliability and stability under different pH conditions.

I. COMPARISONS OF PH SENSORS BASED ON DIFFERENT STRUCTURES

This study collected recent research on pH sensors and compared the sensing performance with the proposed pH sensor, as shown in Table 3. The flexible pH sensor we proposed exhibited a maximum average sensitivity of 46.48 mV/pH and a linearity of 0.996. This sensor demonstrated excellent reliability and sensing performance. Mishra et al. [36]. developed a multifunctional sensor based on an EGFET

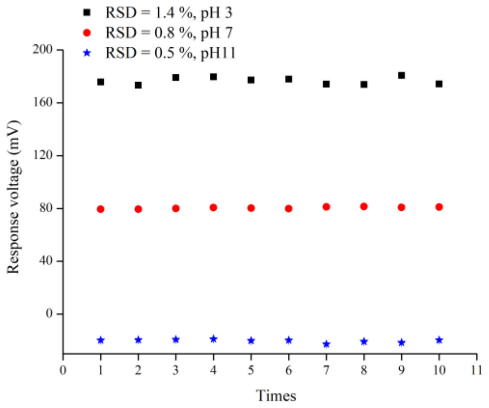

FIGURE 12. The stability of the sensing electrode.

TABLE 3. Comparisons of the sensing performances based on pH sensors with different structures.

Sensing Layer	Sensor Structure	Fabricated Method	Linear Range (pH)	Average Sensitivity (mV/pH)	Linearity	Drift Rate (mV/hr)	Ref.
MgO film	FPCB	RF Sputtering	3-11	46.48	0.996	1.64 (pH 5) 0.88 (pH 9)	This work
CuO NWs	EGFET	Etching and Heating	2-12	48.34	0.998	2.50	2020 [36]
ZnO film	EGFET	Hydrothermal	4-10	34.82	0.992	N/A	2019 [37]
ZnO film	ISFET	RF Sputtering	2-12	42.45	0.972	1.78	2014 [38]
AlN film	ISFET	DC Reactive RF Sputtering	4-10	33.0	0.981	N/A	2019 [39]

structure with CuO nanowires for pH and glucose sensing. The pH sensor had a sensitivity of 48.34 mV/pH and showed good long-term stability with a drift rate of only 2.5 mV/hr. Young et al. [37]. manufactured a low-cost ZnO pH sensor using a hydrothermal method, which exhibited outstanding repeatability and reproducibility. The sensor had a sensitivity of 34.82 mV/pH and a linearity of 0.992. Kao et al. [38]. fabricated a ZnO pH sensor on a silicon substrate with high sensitivity and low drift. Additionally, this sensor could be used for various detections, including Na^+, K^+, glucose, and urea. Sinha et al. [39]. introduced an ISFET pH sensor based on AlN film, which exhibited a sensitivity of 33 mV/pH after measurement and analysis at pH values of 4, 7, and 10. Finally, compared to the pH sensors mentioned above, our proposed flexible pH sensor offers the advantage of flexibility in its structure and demonstrates comparable capabilities.

IV. CONCLUSION

In conclusion, this study has successfully proposed and developed a pH sensor utilizing a MgO film as the sensing layer. The integration of this MgO sensing layer onto an ENIG electrode, which is incorporated into an FPCB, provides several advantages, including flexibility, acid resistance, heat resistance, and cost-efficiency. The performance of the pH sensor was further improved through the modification of the sensing layer with Nafion and APTES. Employing the potentiometric method, the study assessed the performance of the pH sensor, achieving a

measurement range from pH 3 to pH 11, with an average sensitivity of 46.48 mV/pH and an impressive linearity of 0.996. In addition, the pH sensor also has a lower drift rate. To verify the quality of the MgO film, material analysis was conducted using AFM and EDX to examine the surface morphology and elemental composition of the sensing layer. These findings demonstrate the feasibility and potential for the proposed pH sensor as a reliable and effective tool for pH measurement and analysis.

REFERENCES

[1] L. Manjakkal, D. Szwagierczak, and R. Dahiya, "Metal oxides based electrochemical pH sensors: Current progress and future perspectives," *Prog. Mater. Sci.*, vol. 109, Apr. 2020, Art. no. 100635.

[2] M. Futagawa, T. Iwasaki, H. Murata, M. Ishida, and K. Sawada, "A miniature integrated multimodal sensor for measuring pH, EC and temperature for precision agriculture," *Sensors*, vol. 12, no. 6, pp. 8338–8354, Jun. 2012.

[3] A. U. Alam et al., "Polymers and organic materials-based pH sensors for healthcare applications," *Prog. Mater. Sci.*, vol. 96, pp. 174–216, Jul. 2018.

[4] M. Alizadeh-Sani, E. Mohammadian, J. W. Rhim, and S. M. Jafari, "pH-sensitive (halochromic) smart packaging films based on natural food colorants for the monitoring of food quality and safety," *Trends Food Sci. Technol.*, vol. 105, pp. 93–144, Nov. 2020.

[5] C. Dincer et al., "Disposable sensors in diagnostics, food, and environmental monitoring," *Adv. Mater.*, vol. 31, no. 30, May 2019.

[6] S. Sinha and T. Pal, "A comprehensive review of FET-based pH sensors: Materials, fabrication technologies, and modeling," *Electrochem. Sci. Adv.*, vol. 2, no. 5, Oct. 2022, Art. no. e2100147.

[7] A. Gaddour, W. Dghais, B. Hamdi, and M. Ben Ali, "Temperature compensation circuit for ISFET sensor," *J. Low Power Electron. Appl.*, vol. 10, no. 1, p. 2, Jan. 2020.

[8] T.-M. Pan, Y.-H. Huang, J.-L. Her, B.-S. Lou, and S.-T. Pang, "Solution processed $ZnIn_xO_y$ sensing membranes on flexible PEN for extended-gate field-effect transistor pH sensors," *J. Alloys Compd.*, vol. 822, May 2020, Art. no. 153630.

[9] C. H. Kao et al., "Multianalyte Mg-doped InGaZnO electrolyte-insulator-semiconductor biosensors and multiple material characterizations of membrane nanostructures," *IEEE Sensors J.*, vol. 20, no. 18, pp. 10653–10663, Sep. 2020.

[10] P.-H. Yang, Y.-S. Chang, and C.-T. Chan, "Aluminum-doped zinc oxide enzymatic dopamine biosensor integrated with potentiometric readout circuit board," *IEEE Sensors J.*, vol. 23, no. 3, pp. 1809–1817, Feb. 2023.

[11] M. K. M. Arshad, I. Ahmad, A. Jalar, and G. Omar, "The surface characteristics of under bump metallurgy (UBM) in electroless nickel immersion gold (ENIG) deposition," *Microelectron. Rel.*, vol. 46, nos. 2–4, pp. 367–379, Feb.–Apr. 2006.

[12] E. Tanumihardja, W. Olthuis, and A. Van den Berg, "Ruthenium oxide nanorods as potentiometric pH sensor for organs-on-chip purposes," *Sensors*, vol. 18, no. 9, p. 2901, Sep. 2018.

[13] W.-D. Huang, H. Cao, S. Deb, M. Chiao, and J. C. Chiao, "A flexible pH sensor based on the iridium oxide sensing film," *Sens. Actuators A, Phys.*, vol. 169, no. 1, pp. 1–11, Sep. 2011.

[14] D. Srikanya, A. M. Bhat, and C. Sahu, "Design and analysis of high-performance double-gate ZnO nano-structured thin-film ISFET for pH sensing applications," *Microelectron. J.*, vol. 137, Jul. 2023, Art. no. 105811.

[15] C.-C. Yang, K.-Y. Chen, and Y.-K. Su, "TiO_2 nano flowers based EGFET sensor for pH sensing," *Coatings*, vol. 9, no. 4, p. 251, Apr. 2019.

[16] Y. Wan et al., "Conductive and stable magnesium oxide electron-selective contacts for efficient silicon solar cells," *Adv. Energy Mater.*, vol. 7, no. 5, Nov. 2017, Art. no. 1601863.

[17] J. Jeevanandam, Y. S. Chan, and Y. H. Ku, "Aqueous eucalyptus globulus leaf extract-mediated biosynthesis of MgO nanorods," *Appl. Biol. Chem.*, vol. 61, no. 2, pp. 197–208, Apr. 2018.

[18] Y. Furukawa, K. Kitamura, S. Takekawa, A. Miyamoto, M. Terao, and N. Suda, "Photorefraction in $LiNbO_3$ as a function of [Li]/[Nb] and MgO concentrations," *Appl. Phys. Lett.*, vol. 77, no. 16, pp. 2494–2496, Oct. 2000.

[19] C. H. Kao et al., "Magnesium oxide (MgO) pH-sensitive sensing membrane in electrolyte-insulator-semiconductor structures with CF_4 plasma treatment," *Sci. Rep.*, vol. 7, no. 1, p. 7185, Aug. 2017.

[20] S. Chatterjee, M. Saxena, D. Padmanabhan, M. Jayachandra, and H. J. Pandya, "Futuristic medical implants using bioresorbable materials and devices," *Biosens. Bioelectron.*, vol. 142, Oct. 2019, Art. no. 111489.

[21] P.-H. Yang, Y.-S. Chang, and C.-T. Chan, "ZnO and AZO film potentiometric pH sensors based on flexible printed circuit board," *Chemosensors*, vol. 10, no. 8, p. 293, 2022.

[22] W. R. Carmody, "Easily prepared wide range buffer series," *J. Chem. Educ.*, vol. 38, no. 11, pp. 559–560, Nov. 1961.

[23] Y. Cheng et al., "Mechanism and optimization of pH sensing using SnO_2 nanobelt field effect transistors," *Nano Lett.*, vol. 8, no. 12, pp. 4179–4184, Dec. 2008.

[24] Y. Liang, J. Huang, P. Zang, J. Kim, and W. Hu, "Molecular layer deposition of APTES on silicon nanowire biosensors: Surface characterization, stability and pH response," *Appl. Surf. Sci.*, vol. 322, pp. 202–208, Dec. 2014.

[25] S. P. Shylendra, M. Wajrak, K. Alameh, and J. J. Kang, "Nafion modified titanium nitride pH sensor for future biomedical applications," *Sensors*, vol. 23, no. 2, p. 699, Jan. 2023.

[26] T. Hiemstra, W. H. Van Riemsdijk, and G. H. Bolt, "Multisite proton adsorption modeling at the solid/solution interface of (hydr) oxides: A new approach: I. Model description and evaluation of intrinsic reaction constants," *J. Colloid Interface Sci.*, vol. 133, no. 1, pp. 91–104, Nov. 1989.

[27] P. Bergveld, "Thirty years of ISFETOLOGY: What happened in the past 30 years and what may happen in the next 30 years," *Sens. Actuators B, Chem.*, vol. 88, no. 1, pp. 1–20, Jan. 2003.

[28] R. E. G. Van Hal, J. C. T. Eijkel, and P. Bergveld, "A general model to describe the electrostatic potential at electrolyte oxide interfaces," *Adv. Colloid Interface Sci.*, vol. 69, nos. 1–3, pp. 31–62, Dec. 1996.

[29] Y. Jia et al., "Role of sodium hexametaphosphate in MgO/SiO_2 cement pastes," *Cement Concr. Res.*, vol. 89, pp. 63–71, Nov. 2016.

[30] L. F. Amaral, I. R. Oliveira, R. Salomão, E. Frollini, and V. C. Pandolfelli, "Temperature and common-ion effect on magnesium oxide (MgO) hydration," *Ceram. Int.*, vol. 36, no. 3, pp. 1047–1054, Apr. 2010.

[31] O. Fruhwirth, G. W. Herzog, I. Hollerer, and A. Rachetti, "Dissolution and hydration kinetics of MgO," *Surf. Technol.*, vol. 24, no. 3, pp. 301–317, Mar. 1985.

[32] L. Fu, C. Ybert, O. Bonhomme, L. Joly, and A.-L. Biance, "Electrokinetic sweeping of colloids at a reactive magnesium oxide interface," *Soft Matter*, vol. 17, no. 38, pp. 8705–8711, Sep. 2021.

[33] J.-C. Chou et al., "Study of the glucose sensor based on potentiometric non-enzymatic nafion/CZO thin film," *IEEE Sensors J.*, vol. 21, no. 14, pp. 15926–15934, Jul. 2021.

[34] J.-F. Cheng, J.-C. Chou, T.-P. Sun, S.-K. Hsiung, and H.-L. Kao, "New calibration methods to eliminate the non-ideal effect of drift and hysteresis in all-solid-state potassium electrode," *IEEE Sensors J.*, vol. 11, no. 5, pp. 1263–1273, May 2011.

[35] S. Jamasb, S. Collins, and R. L. Smith, "A physical model for drift in pH ISFETs," *Sens. Actuators B, Chem.*, vol. 49, nos. 1–2, pp. 146–155, Jun. 1998.

[36] A. K. Mishra, D. K. Jarwal, B. Mukherjee, A. Kumar, S. Ratan, and S. Jit, "CuO nanowire-based extended-gate field-effect-transistor (FET) for pH sensing and enzyme-free/receptor-free glucose sensing applications," *IEEE Sensors J.*, vol. 20, no. 9, pp. 5039–5047, May 2020.

[37] S.-J. Young, L.-T. Lai, and W.-L. Tang, "Improving the performance of pH sensors with one-dimensional ZnO nanostructures," *IEEE Sensors J.*, vol. 19, no. 23, pp. 10972–10976, Dec. 2019.

[38] C. H. Kao et al., "Multianalyte biosensor based on pH-sensitive ZnO electrolyte–insulator–semiconductor structures," *J. Appl. Phys.*, vol. 115, no. 18, May 2014, Art. no. 184701.

[39] S. Sinha, R. Mukhiya, R. Sharma, P. K. Khanna, and V. K. Khanna, "Fabrication, characterization and electrochemical simulation of AlN-gate ISFET pH sensor," *J. Mater. Sci. Mater. Electron.*, vol. 30, pp. 7163–7174, Apr. 2019.

PO-HUI YANG (Member, IEEE) was born in Tainan, Taiwan, in 1965. He received the B.Eng. degree in marine electronics engineering from National Taiwan Ocean University, Keelung, Taiwan, in 1993, the M.S. degree in industrial education from National Taiwan Normal University, Taipei, Taiwan, in 1995, and the Ph.D. degree from the Institute of Electrical Engineering at National Chung Cheng University, Chiayi, Taiwan, in 2002. From 2001 to 2003, he was an Assistant Professor with the Department of Electronics, Southern Taiwan University of Science and Technology. From 2003 to 2004, he was a High-Performance Digital IC Design Engineer and Circuit Design Section Manager with the SoC Technology Center, Industrial Technology Research Institute, Hsin-Chu, Taiwan. In 2004, he joined the Department of Electronic Engineering, National Yunlin University of Science and Technology, where he is currently an Associate Professor. His research interests include high-speed and low-power CMOS IC design, advanced IC packaging, and low-power biosensor IC design.

JYUN-MING HUANG was born in Chiayi, Taiwan, in October 1999. He received the bachelor's degree from the Department of Electronic Engineering, Kun Shan University, Tainan, Taiwan, in 2022. He is currently pursuing the master's degree with the Graduate School of Electronic Engineering, Nation Yunlin University of Science and Technology. His research interests include analog readout circuits and integrated circuits for biosensor measurement systems.

YING-SHENG CHANG was born in Taoyuan, Taiwan, in February 1999. He received the bachelor's and M.S. degrees from the Department of Electronic Engineering, National Yunlin University of Science and Technology, Taiwan, in 2020 and 2022, respectively. His research interests include analog readout circuits and temperature compensation circuits for biosensor measurement systems.

CHE-TSUNG CHAN was born in Taichung, Taiwan, in November 1998. He received the bachelor's and M.S. degrees from the Department of Electronic Engineering, National Yunlin University of Science and Technology, Taiwan, in 2020 and 2022, respectively. His research interests include analog circuits for biosensors and digital glitch cancellation circuits.

WEI-SHUN CHEN was born in Taiwan, in December 1999. He received the bachelor's degree from the Department of Aeronautical Engineering, National Formosa University. He is currently pursuing the master's degree with the Graduate School of Electronic Engineering, National Yunlin University of Science and Technology. His current research area is biosensor applications.